C. R. Mecanique 339 (2011) 518–531

Contents lists available at ScienceDirect

Comptes Rendus Mecanique

www.sciencedirect.com

Surface mechanics: facts and numerical models

Analysis methods and size effects in the indentation fracture toughness assessment of very thin oxide coatings on glass

Steve J. Bull

Newcastle University, School of Chemical Engineering and Advanced Materials, Newcastle upon Tyne, NE1 7RU, UK

ARTICLE INFO

Article history:
Available online 21 June 2011

Keywords:
Nanoindentation
Fracture
Toughness
Oxide coatings
Glass

ABSTRACT

Very thin oxide coatings (< 100 nm) which are used as anti-reflection and barrier layers in low emissivity architectural glass have been studied by nanoindentation methods to determine the effect of coating thickness on fracture toughness. Traditional microindentation-derived methods to determine the fracture toughness are unsuitable for assessing very thin coatings (< 500 nm) and alternative energy-based models are required depending on what features are visible in indentation load–displacement curves. In cases where radial cracks are formed and grow in a discontinuous manner there are excursions in the load–displacement curve which can be the basis for analysis. In cases where picture frame cracks are observed there are no such features and an alternative approach based on assessment of irreversible work of indentation is required. This paper reviews the methods for obtaining fracture toughness data for very thin coatings and assesses the existence of size effects in the mechanical response of oxide coatings with different thickness on a glass substrate. For oxide coatings in the thickness range 100 to 400 nm no size effects in fracture toughness were observed.

1. Introduction

For bulk materials and sufficiently thick coatings standard methods to measure toughness have been established including methods requiring the manufacture of standard test pieces which can be machined from the bulk or indentation methods which are often easier to perform but give more scattered results (e.g. [1,2]). The main testing methodologies for the assessment of bulk materials and thick coatings include bending, buckling, tensile, indentation, and scratch tests. As coating thickness is reduced and complex compositions and structures are introduced, it is difficult to use standard mechanical test methods to measure the fracture toughness and indentation-based methods are preferred. However, it is not always straightforward to extract toughness information for a given coating/substrate system and different analysis methods have been developed which are suitable for application in different circumstances as there is no universally applicable approach. Techniques which are used to estimate the coating toughness can be divided into two main categories; stress analysis methods, and energy based methods. This paper summarises and compares these methods in order to facilitate the selection of an appropriate approach to measure the toughness of coatings on architectural glass.

For electronic and optical applications the design of coating-substrate systems has been predominantly controlled by their functional properties but more recently the mechanical response of the system has been used to enhance functional properties, as in the case of low emissivity coatings on architectural glass where scratch and damage resistance is a critical parameter in successful handling. As coatings become more complex, with multilayer and graded architectures now in widespread use, it is very important to obtain the mechanical properties (such as hardness, elastic modulus, fracture

E-mail address: s.j.bull@ncl.ac.uk.

1631-0721/$ – see front matter
doi:10.1016/j.crme.2011.05.009

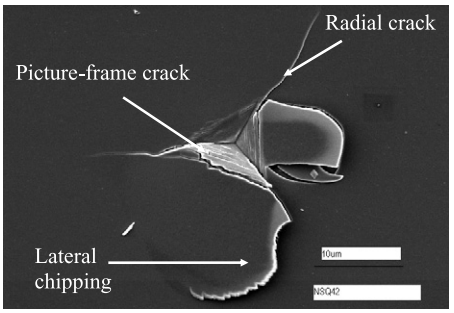

Fig. 1. Scanning electron micrographs of a Berkovich indentation in SiC on silicon showing radial and lateral fracture as expected from the behaviour of the silicon substrate and picture frame cracking in the coating itself.

toughness, etc.) of individual coating layers for use in design calculations at the thickness present in the coating design since size-effects may be important in very thin layers (<1 μm). Nanoindentation testing is often the only viable approach to assess the damage mechanisms and properties of such very thin coatings since it can operate at the required scale and provides fingerprint of the indentation response of the coating/substrate system. If coating properties are to be assessed, the key point is to ensure any measured value is free from the influence of the deformation of the substrate or lower coating layers. Finite element analysis of indentation load displacement curves can be used to extract materials properties for design; as coating thicknesses decrease it is observed that the yield strength required to fit the curves increases and scale-dependent materials properties are essential for design. However, for oxide coatings on architectural glass there is also a need to determine if there are size effects in fracture as well as plasticity and this is the subject of this paper.

2. Indentation fracture in bulk materials and coatings

2.1. Sharp versus blunt contact

In order to generate fracture in an indentation test it is usual to press an indenter against the surface of the test material under an increasing load. For bulk materials, the precise form of fracture will depend on the geometry of the indenter and whether there is a transition from elastic to elastic–plastic behaviour during the loading cycle. For sharp indenters, very high shear stresses are developed below the indenter and plastic deformation initiates below the contact at a relatively low load, usually well before the onset of fracture [1]. As the load increases an approximately hemispherical plastically deforming zone develops around the contact. At higher loads still the wedging action of the cone generates a median vent crack below the surface; for real faceted indenters these cracks are often initiated parallel to indenter edges but may also form with other orientations due to microstructural or crystallographic effects. In some tougher systems (e.g. WC/Co) surface radial cracks may develop on loading in the absence of a median crack (Palmqvist cracks). These are generally initiated at stress concentrations on the indenter edges. On unloading, the median cracks extend to the surface making a half penny (semicircular) radial crack extending well outside the indentation impression – it is analysis of this crack system which is often the basis of toughness determination (Fig. 1). On unloading, the elastic depression of the surface is relaxed but, due to the formation of the plastic zone beneath the indenter, this relaxation is restricted and residual stresses are set up around the impression. Tensile stresses at the elastic–plastic boundary beneath the indenter can lead to the initiation of a lateral crack which propagates parallel to the surface initially but may divert to the surface and lead to chipping.

The stresses responsible for fracture are critically dependent on the angle of the indenter, with acute angles leading to higher stresses and a higher chance of fracture. For this reason workers intending to introduce fracture into a material during nanoindentation tests tend to use the sharper cube corner indenter, rather than the usual Berkovich indenter which is commonly used for hardness assessment as it displaces a similar volume of material as the traditional Vickers indenter at a given penetration depth.

2.2. Fracture of coatings

For coating/substrate systems two types of cracking may be observed which are useful in assessing coatings properties:

1. Through-thickness fracture – useful for coating toughness assessment
2. Interfacial detachment – useful for adhesion assessment

Assessment of the toughness of coatings is generally based on fracture patterns which are confined to the coating itself. For very thick coatings the same approaches as are used for bulk materials based on the formation of well-developed radial cracks can be applied (Fig. 2a). Typically such cracks are at least 5–10 μm in length (from the centre of the impression to the crack tip) which generally restricts the approach to coatings in excess of 10 μm thick where no significant elastic or plastic deformation of the substrate occurs prior to coating fracture.

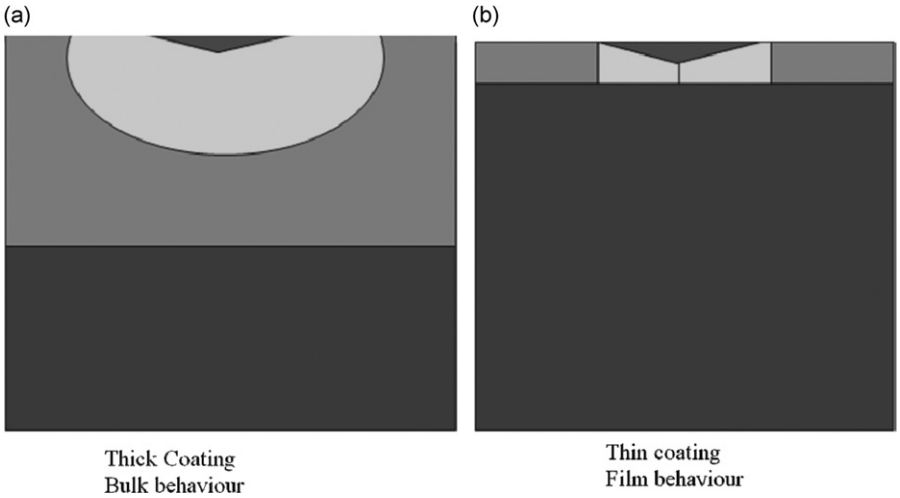

Fig. 2. Schematic cross-section of contact-induced fracture patterns around a sharp indenter (a) thick coating/bulk behaviour and (b) thin coating behaviour.

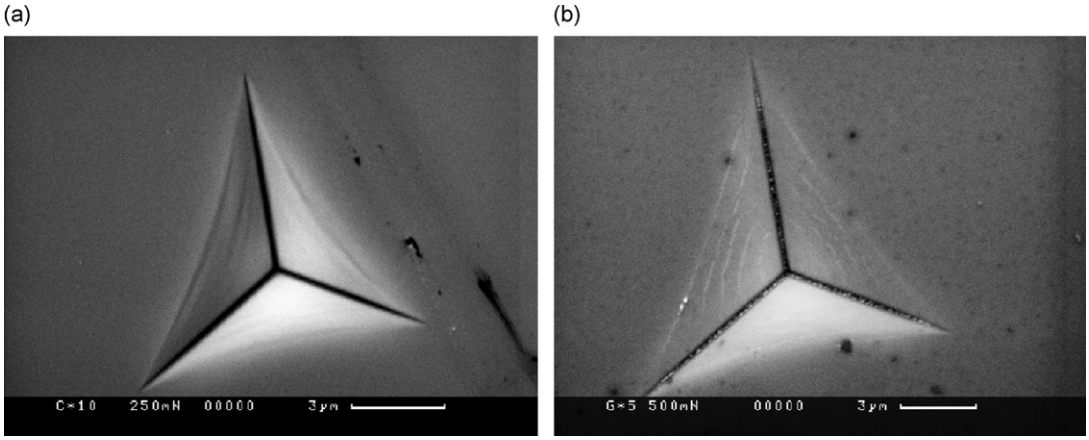

Fig. 3. Through-thickness fracture within hardness impressions in architectural glass coated with a solar control coating architecture (a) radial and (b) picture frame cracking.

For very thin coatings, elastic and plastic deformation of the coating and substrate cannot be ignored and the through-thickness fracture events are generally confined within the impression (Fig. 2b). For a sharp Berkovich indenter the following crack sequence is observed. Initially the contact is elastic, but the coating is bent to conform to the shape of the indenter, a process which can be exacerbated by plastic deformation of the substrate. Regions of maximum tensile stress are generated at the surface at the edge of the impression and beneath the indenter at the coating substrate interface. The stress beneath the indenter acts over a greater area and generates radial cracks which propagate to the surface and along the indenter edges but do not generally leave the impression (Fig. 3a). As the load increases, the stresses at the edge of the impression are large enough to generate picture frame cracking delineating the edge of the impression (Fig. 3b). Further increases in load will increase the size of the impression leading to discontinuous growth of radial cracks and the formation of nested arrays of picture frame cracks.

Having identified which crack patterns occur it is necessary to measure crack dimensions and then select an appropriate analysis method if the toughness is to be determined. This is discussed in the next section.

3. Approaches to assess the fracture toughness of coatings

3.1. Stress analysis based models

Empirical observations usually find that the toughness (K_{IC}) of the indented materials is proportional to the applied load P divided by the radial crack length, c, raised to the power of 1.5 during indentation by a Vickers indenter. Combining stress

analysis for the model of the analogous expanding spherical cavity problem and simplistic dimensional analysis, Lawn and Evans [1] developed the following expression to assess the toughness of ceramics and glass,

$$K_{IC} = \chi P/c^{3/2} = \xi_v^R (E/H)^m P/c^{3/2} \tag{1}$$

where is ξ_v^R a calibration coefficient which depends on indenter geometry and crack patterns and m is a constant (usually $m = 1/2$). For well developed radial cracking produced by a Vickers or Berkovich indenter comparison of the indentation results and bulk toughness measurement techniques allow the constant to be determined empirically. It can be shown that $\xi_v^R = 0.016 \pm 0.004$ [2] but there is considerable uncertainty in the constant itself, leading to inherent uncertainty in the deduced toughness. For median crack, the coefficient ξ_v^R will be lower for bulk materials [1] and coatings [3] which may imply that median cracks tend to occur at higher loads. This was confirmed by Cook and Pharr [4]. As the semi-angle of the indenter decreases, ξ_v^R increases since $\xi_v^R \sim (\cot\varphi)^{2/3}$ [1,5]. Such geometry dependent phenomena have been verified for different tip angles from 35.3° to 75° [5].

E and H can be easily measured from an indentation load–displacement curve and the crack length c can be determined by scanning electron microscopy (SEM), atomic force microscopy (AFM) or reflected light micrographs. The simplicity and reliability of this method leads its wide application. However, it requires the crack to be sufficiently developed (i.e. $c \gg 2a_c$, where a_c is the radius of the impression) which accordingly requires a relatively high load. For bulk materials there can be considerable point to point variations in the toughness measured using indentation methods and the test should be repeated many times to get good data (the average value obtained from at least 40 radial cracks from a minimum of ten impressions is often required) which can be time consuming. For thin films, high loads generate large indenter penetrations which may result in significant deformation of the substrate. In such cases, the initial residual stress field to drive the fracture may be disturbed by the interface and substrate so that the fracture shape will also change, which reduces the reliability of the method.

Harding et al. [6] found that using sharper tip such as a cube corner tip could dramatically lower the threshold load for cracking. At the same load, a cube corner tip stresses a larger volume of material than a Berkovich indenter (by more than 3 times) which leads to a much higher stress intensity. It has been proposed that the cube corner indenter could reduce the critical load for fracture by more than 10 times for most brittle materials [7]. In addition to the advantage of reducing critical load, at the same penetration the more confined plastic deformation compared to Berkovich indenter is also a merit of the cube corner tip which could eliminate the influence from the substrate [8]. Therefore, it is preferred to use a cube corner tip when assessing the toughness of thin films (e.g. [6,7,9,10]). However, different researchers have reported different values for the coefficient ξ_v^R for a cube corner tip in Eq. (1). If we assume that ξ_v^R is related to tip angle only, it can be expected to have the value of 0.0369 based on the agreed value for the Berkovich indenter. However a range of values are reported in the literature which sometimes differ from this value considerably; e.g. 0.0319 [11], 0.036 [6], 0.04 [7] and 0.0535 [12]. The different calibration materials used may be a very important factor in this variation [13]. When the contact scales down to submicrometer dimensions, measurement errors and indenter tip radius and flaw distribution are also important.

As suggested by Anstis et al. [2] and Lawn et al. [1], Eq. (1) does not take into account pile-up or sink-in around the impression. For many ceramics which have high H/E (~ 0.1) sink-in occurs during nanoindentation but this has a small effect on the measured toughness. However, pile-up tends to occur in materials with low H/E (< 0.05) which show extensive plastic deformation during indentation and are not likely to fracture. Even if fracture does occur for these materials the toughness values determined are likely to be in considerable error due to the effects of significant pile-up. Both pile-up and sink-in will alter the crack dimension and shape, and may also influence the residual stress field. Thus, the different extent of sink-in and pile-up between different calibration materials may cause the discrepancy in the constant for Eq. (1) as well. Another possible reason is that the flaw size and distribution may significantly vary in different materials; when the indenter becomes sharper, individual defects play a vital role in the fracture mechanism when the stressed volume is small. In addition, when indenting the hard materials the sharp tip is much easier to wear or even break leading to short indenter life which is a very important issue when making indentations by a cube corner tip.

Although some problems exist, Eq. (1) has been widely been used to estimate the toughness of relatively thick coatings (>10 μm).

Due to the mismatch in properties between coatings and substrates, and the deposition conditions used in different coating techniques, it is almost inevitable that residual stress will be induced in the coating which is not be considered in Eq. (1). The residual stress item may be ignored for a very tough material but it becomes significant for materials with low toughness (e.g. sol-gel coatings [3,14]). In order to solve this problem, a modified expression considering residual stress, σ (can be pre-existing surface stress in bulk materials or the residual stress in coatings) has been suggested [14–17],

$$K_c = \xi_v^R (E/H)^{1/2} P/c^{3/2} + 2\sigma (c/\pi)^{1/2} \tag{2}$$

It should be noted that the constant π assumes a well-developed half-penny crack but it can be expected that the both the stress field and crack shape will be disturbed by the substrate. Malzbender et al. [14] argued that the radial cracks are mainly confined to the surface of a coating so that the influence of substrate on the stress field can be ignored. This assumption was proved to be valid in their relatively thick coatings (2 μm and 4 μm in thickness in Ref. [14]). Plotting $\xi_v^R (E/H)^{1/2} P/c^{3/2}$ versus $2(c/\pi)^{1/2}$ both toughness (the intercept with the ordinate axis) and residual stress (the slope)

can be obtained. When the substrate effect becomes more important, a shape factor initially defined by [18] is introduced to account for the shape modification which occurs. Eq. (2) is then modified to,

$$K_c = \xi_v^R (E/H)^{1/2} P/c^{3/2} + Z\sigma c^{1/2} \tag{3}$$

where

$$Z = 1.12\sqrt{\pi}\,\frac{d/c}{(3\pi/8) + (\pi/8)(d/c)^2} \tag{4}$$

Here d is the depth of radial crack. For a half penny-like crack, Z equals 1.26 close to the value of 1.13 in Eq. (2). The difference may result from slightly different assumptions of fracture mechanism in the two models. Although it is difficult to accurately measure the crack depth, den Toonder et al. [19] argued that the fracture toughness can be obtained without the knowledge of Z and Z is only important when determining the residual stress.

This method works well for coatings with significant residual stress and low toughness such as organic–inorganic hybrid coatings with thickness of more than 3 μm on glass [3] and SiO_2-filled methyltrimethoxysilane coatings with thickness of more than 2 μm on glass [14]. Otherwise, the scatter in $\xi_v^R (E/H)^{1/2} P/c^{3/2}$ and $2(c/\pi)^{1/2}$ leads to poor quality fits to Eq. (3).

Many of the most successful applications of this approach are for hard coatings on a hard substrate. If harder coatings are deposited on a softer substrate (e.g. harder ceramics on glass, ceramics on metals or polymers), plastic deformation of the substrate may occur during the propagation or even during the initiation of the radial crack in the coating and an additional bending stress will be imposed on coating which totally changes the fracture mechanism which Eqs. (1)–(3) rely on. Thus, the mismatch between coatings and substrate will influence the stress field when it propagates into interface and substrate and models based on radial cracking become invalid.

Furthermore, when the coating thickness decreases, well-developed radial cracking is no longer observed (e.g. 400 nm Solar control coatings on glass in Ref. [8]; 500 nm SiO_2-filled methyltrimethoxysilane coatings on glass in [3]). In such cases, the utility of the approach will be in doubt. For example, Laugier [20] and Nihara [21] reported that the linear scaling relation between K_{IC} and $P/c^{3/2}$ stopped when $c < 2.5a_c$. However, Jang et al. [5] argued that such a scaling relationship is still maintained even for small cracks in Si (100). Scholz et al. [22] found that such a scaling relationship remained even when the radial crack length was down to $1.1a_c$ for typical ceramics such as fused silica, sapphire etc.

For a radial crack confined within the contact region, Tanaka et al. [23] argued that the coefficient in Eq. (1) should be bigger if the crack was not sufficiently developed. Extrapolating the results of Scholz et al. [22], a smaller coefficient can be expected. These differences between research workers demonstrate that the accuracy Eq. (1) is influenced by contact scale, microstructure and materials properties. Alternatively, for subthreshold cracking, a model relating the toughness to the hardness and strength of the materials has been suggested [24] which gives reasonable results for common brittle materials such as soda-lime glass, Si and sapphire. The disadvantage is that the constants in the model are empirical, varying with materials [see more details in Ref. [24].

If it is assumed that Eq. (1) holds for small crack lengths (i.e. $c > a_c$, but not much bigger), the difficulty to accurately measure crack length is an issue so a method to estimate crack length in the absence of any imaging system was suggested by Field et al. [25] based on the concept of crack opening displacement and utilising the feature of a pop-in in the load–displacement curve. For a typical pyramidal indenter, the crack opening displacement (COD) δ_{COD} can be given by,

$$\delta_{COD} = 2h_{ex} \cot\varphi \tan 30^\circ \tag{5}$$

where ϕ is face-to-centre angle and h_{ex} is the extra penetration caused by entry of the indenter into the crack. Field et al. [25] suggested that h_{ex} can be estimated as the difference between the actual displacement with pop-in and the extrapolated displacement without pop-in (i.e. h_{m2}–h_{m1} as depicted in Fig. 4).

By geometrical analysis for a pyramidal indenter with crack length c, the distance from crack tip to indentation centre is given by,

$$c = (h_{m2} - h_{ex}) \cot\varphi + \frac{\pi E_r h_{ex} \cot\varphi \tan 30^\circ}{4pD} \tag{6}$$

where E_r is the reduced elastic modulus; p is the pressure at the centre of crack, and D is a constant. Since p is likely to be proportional to the Meyer's hardness [26], Eq. (6) can be rewritten as follows,

$$c = h_{m2} \cot\varphi + \left(Q\,\frac{E_r}{H_M} - 1\right) h_{ex} \cot\varphi \tag{7}$$

Here Q is a combined constant which can be obtained by fitting the relationship between c and h_{ex}. Reasonable results are reported and it was found that Q was similar (with difference of $\sim 10\%$) for two different materials in Ref. [25]. Although it is not completely justified, assuming that the value of Q is constant allows this method to be used for other bulk materials whose cracks are not easily measured even at high stress intensity which avoids the time consuming work in imaging the cracks. Further, it allows us to calculate the threshold conditions for radial cracking if forming the crack did not significantly delay the pop-in. However, data obtained by this method is highly scattered, particularly for fused silica. For materials that have significant densification below the indenter, the residual stress levels adjacent to indenter will be reduced thus leading

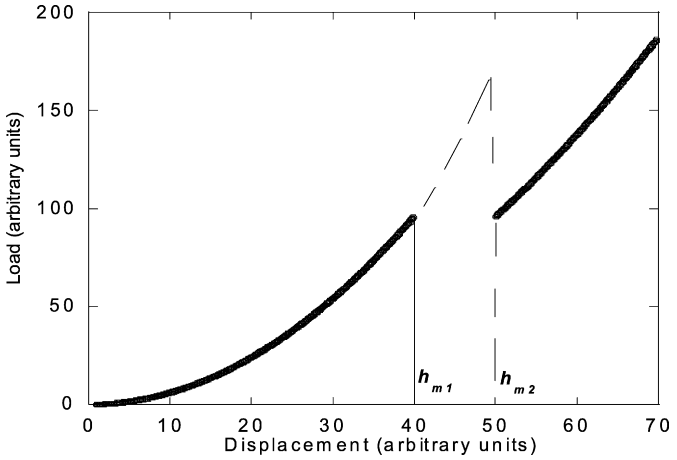

Fig. 4. Schematic of pop-in in a load–displacement curve obtained under load control conditions.

to a decrease of crack length. A conventional indentation method based on measurement of radial crack geometry will result in gross over-prediction of fracture toughness [27]; unfortunately, fused silica falls into this category [2].

Another important issue is the interaction between different crack systems. It is possible that a cone crack appears prior to radial/median cracking and this provides a confining boundary for the development of radial or median cracks. Also it is possible that a lateral crack will accompany radial cracks and the expansion of lateral cracking will confine the propagation of the radial cracks. For some coated systems with relatively poor adhesion, delamination at the interface may be associated with radial fracture in coatings before the radial crack is well-developed which will seriously affect the residual stress field to drive the radial crack and the dimensions of radial fracture. In such cases, Eqs. (1)–(3) become invalid or at least less reliable. Further, for some coated systems indented by a Berkovich indenter at high load, only cone cracks or picture-frame cracks were observed (e.g. [28]), in which case, the models above cannot work.

The crack opening displacement can be empirically correlated to the fracture toughness of a range of materials [29, 30]. Based on linear elastic fracture mechanics, the near-tip stress intensity K_{tip} for a crack related to the crack open displacement (COD) is given by [29]

$$u(r) = \frac{4K_{tip}b^{1/2}}{\pi E_r}\left[A\left(1-\frac{r}{c}\right)^{1/2} + B\left(1-\frac{r}{c}\right)^{3/2} + C\left(1-\frac{r}{c}\right)^{5/2}\right] \tag{8}$$

where r, a and c are the radial position of crack tip, contact radius, and crack length, respectively, as measured from the indent centre. Here the constants A, B, C are given by,

$$\begin{aligned} A &= \left(\frac{\pi a}{2b}\right)^{1/2} \\ B &\approx 0.011 + 1.8179\ln\frac{a}{b} \\ C &\approx -0.6513 + 2.121\ln\frac{a}{b} \end{aligned} \tag{9}$$

As traditionally assumed, K_{tip} can be regarded as the material's fracture toughness since the crack is supposed to arrest under such conditions.

Conventional indentation methods exhibit R-curve behaviour (i.e. increasing toughness with crack length) because of extrinsic toughening mechanisms such as crack bridging [31]; such effects can be separated out by using the COD method. Since the approach does not depend on knowledge of the hardness, unlike CIM, it is not expected to be influenced by indentation size effects (ISE) which are not unusual in ceramics (e.g. [32,33]). The COD method is influenced by secondary radial cracks which release some of residual stress thus affecting the COD of the main radial crack [30]. The COD method will also be influenced by subsurface fracture such as lateral cracking which may reduce the opening displacement of the radial crack. Where radial cracks are not driven by residual stress [4] and indenter geometry [10,25] no stress analysis method developed to date generates satisfactory toughness results.

In order to avoid the problems of cracking confined within the impression, a different COD method was proposed which does not require knowledge of the crack length. It only requires that the crack is in quasi-equilibrium which is the case immediately after indentation with sharp tips [27]. With the aid of the solution of the near-tip displacement field [34], a numerical solution for fracture toughness can be obtained. Reasonable results were reported for soda-lime glass [35]. This method is not affected by densification. However, this method is not suitable for nanoindentation at low loads when the COD is of the order of a few nanometres and measurement uncertainties will dominate the results.

A so-called strength method was also proposed by Chantikul et al. [36] based on indentation which avoids some of the systematic errors in Eq. (1) and eliminates the need for fracture imaging. It combined indentation and strength tests (see details in initial paper [38]) and derived the following expression to determine toughness,

$$K_c = \eta_v^R (E/H)^{1/8} \left(\sigma P^{1/3}\right)^{3/4} \tag{10}$$

and $\eta_v^R = [(256/27)(\pi\Omega)^{3/2}\xi_v^R]^{1/4}$, where Ω is a crack-geometry factor which takes into account free-surface effects, cracking interactions such as the lateral-radial cracking interaction mentioned previously and the deviation from penny-like shape. It can be seen that the constant η_v^R in Eq. (10) still relies on ξ_v^R from Eq. (1), which indicates all the errors contained in ξ_v^R will be introduced into η_v^R. Therefore, it cannot be expected that this method will significantly improve the accuracy of toughness determination compared to Eq. (1). In addition, it requires an indentation at the centre of the prospective tensile face of a bend test specimen and only one result can be obtained for a single specimen, which is a possible reason that the method is not as popular as CIM using Eq. (1). In addition, this method is very difficult to apply to thin coatings. Therefore, it will not be discussed in detail here and interested readers are referred to [36].

Marshall et al. [37] proposed a model to relate the toughness of brittle bulk materials to the depth at which lateral cracks occur and the driving force due to the residual stress during unloading.

$$K_c^4 = \frac{P_0 A_0^2}{\delta_0} (\cot\theta)^{\frac{2}{3}} \frac{H}{E} H^3 \tag{11}$$

where P_0 is the threshold load for lateral cracking, A_0 and δ_0 are dimensionless constants ($A_0 = 3/4$ and $\delta_0 = 1200$) and θ is the half-included angle for the indenter [35]. With the aid of the continuous recording of load and displacement, a feature of instrumented indentation, this method can be simply applied to relatively thick coated systems when the lateral crack is confined within the coating.

In addition to the half-penny (or approximately half-penny) crack patterns, Palmqvist radial cracking was observed for stiff and hard bulk materials such as WC (e.g. [38]). This usually occurs at high load for a much tougher material than glass. Palmqvist cracks tend to appear during loading, initiating at corners due to the high tensile stress intensity and are driven by hoop tensile stress. In this case, the proportional relationship between toughness K_{IC} and $P/c^{1.5}$ as shown in Eq. (1) is still valid, however, the exponent of E/H was found to be $2/3$ and an additional term which correlates to the crack dimension over contact size will affect the proportionality coefficient [39]. It was found that the toughness values of a range of ceramics based on the half-penny cracking pattern and the Palmqvist radial morphology agree to within 10% [39]. Since this kind of crack tends to occur at relatively high load in relatively tough bulk materials, it need not be considered in the assessment of thin coatings due to the intention to eliminate the substrate affect. However, this model can be treated as another explanation for the lower coefficient in Eq. (1) in the case of smaller cracks which is the argument by Scholz et al. as discussed previously.

3.2. Energy based models

3.2.1. Models based on features in the load–displacement curve

All the methods above are stress-field based and usually also require some empirical fitting. As discussed in the previous section, there are many problems and uncertainties inherent in the models, especially when their application is extended to thin films. Therefore, alternative methods have been developed such as the energy based models which will be discussed in this section.

A widely used energy-based model was initially proposed by Li et al. [9,40] based on extrapolating the loading curve when there is a step associated with fracture in it. In this model the load–displacement curve is extrapolated from the step start point (assumed to be the onset of fracture) to its end point, and the difference between the extrapolated curve and the measured curve (i.e. the area ACD in Fig. 5) is regarded as the fracture dissipated energy. For convenience, this method will be denoted as the ld–dp method in this paper. The coating toughness is then given by [40]

$$K_{IC} = \left[\frac{E_f U_{fr}}{(1-\nu^2) A_{crack}}\right]^{\frac{1}{2}} \quad \text{for plane strain mode I fracture} \tag{12}$$

Here U_{fr}, and A_{crack} are the fracture dissipated energy and the fracture area and E_f and ν are Young's modulus and Poisson's ratio of the coating, respectively. The initial model was developed for measure toughness based on a through-thickness ring crack and it was modified by considering the number of cracked segments and the effective coating thickness which accounted for the fact that crack did not propagate perpendicular to the film/substrate interface when assessing the coating toughness from chipping events [19,41].

However, through thickness fracture may change the stress field around the indenter and thus change the elastic–plastic behaviour of the coated system. This influence has been completely ignored in this model. It was also argued elsewhere [19] that the area ACD in Fig. 5 is not the actual energy dissipated by fracture. In addition, this model cannot be equally applied to displacement control experiments when load drops occur in the load–displacement curve.

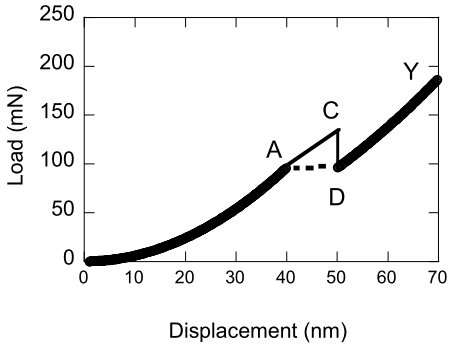

Fig. 5. Schematic of the ld–dp method to determine the fracture dissipated energy, i.e. area ACD. See text.

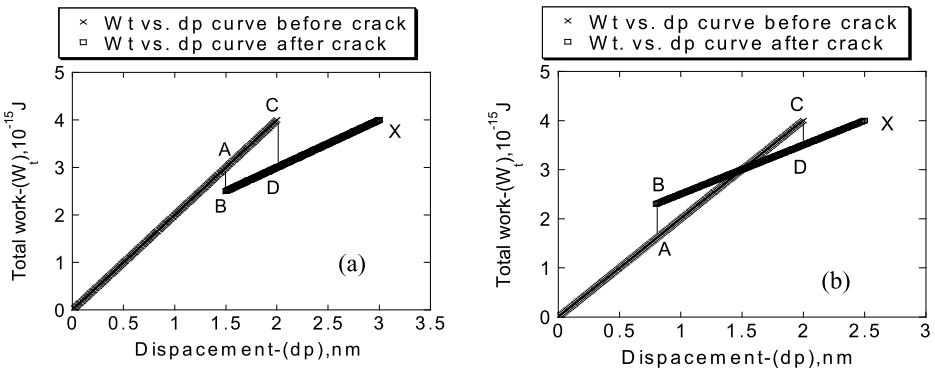

Fig. 6. Schematic of extrapolating the total work vs. displacement curve before and after cracking to determine the fracture dissipated energy CD-AB. Compared to CD, AB can be positive as displayed in (a) or negative as depicted in (b) depending on the actual coated systems (see text).

Therefore, this model was further developed by Chen and Bull [10,42] based on a plot of total work of indentation vs. displacement (W_t–dp) which can be obtained by integrating the load–displacement curve. The method to determine fracture energy is explained in Fig. 6.

First, we extrapolate the initial W_t–dp curve from the cracking start point A to the cracking end point C, to get the work difference CD after fracture; then we extrapolate the W_t–dp curve after cracking (i.e. curve XD in Fig. 6) backward to the cracking start point and thus obtaining the work difference AB at the onset of fracture where point B has the same depth as point A. AB represents the work caused by the different elastic–plastic deformation behaviour of the material before and after fracture whereas CD represents the total work difference caused by the presence of cracking which consists of the change of elastic–plastic deformation behaviour between the uncracked system and cracked system plus the fracture dissipated energy. The difference between the two (i.e. CD minus AB in Fig. 6) will be the fracture dissipated energy.

From a thermodynamics point of view, the change of total Gibbs free energy during a fracture event results from the compliance change of the system, the exchange of elastic strain with plastic strain, and the change in crack area as well as energy losses in any other processes which may occur such as phase changes [43]. The decreases of the compliance of the coating and the change of elastic–plastic strain field of the whole coated system can be additive (see Fig. 6a, for a typical hard coating on a softer substrate) or counteract (see Fig. 6b, for a typical hard coating on a harder substrate) each other depending on the actual coated systems and loading process. It can be shown that for most materials CD-AB will not be zero provided the load drops or plateaux in the load–displacement curve are associated with fracture [8]. This method has been successfully applied to many ceramic coatings on glass, giving energy release rates in the range 16–45 J/m^2 with the corresponding toughness 1.6–2.5 MPa m$^{1/2}$ (see Table 1). For the conventional indentation method (i.e. Eq. (1)), if using a coefficient 0.0319 for a cube corner tip, the toughness which was obtained for all these ceramic coatings was almost identical to the toughness of the substrate glass. As argued in [10,42], the CIM values are not reasonable, in contrast, the results given by W_t–dp model are more sensible.

As predicted previously, the Li method is likely to overestimate the toughness of typical hard and stiff coatings on a hard substrate. For example, it was reported that toughness of a cathodic arc carbon coating on Si determined by the Li method [9,40] was 10.9 MPa m$^{1/2}$ which was higher than the toughness ($\sim$ 7.9 MPa m$^{1/2}$) of bulk diamond [44]. This is not realistic because of the abundant defects in the coating. The W_t–dp method gives a toughness of 5.5 MPa m$^{1/2}$ which is more reasonable. The method has been verified for CN_x coatings (1 μm) on stiffer and harder substrates [40]. Evidence for underestimation of toughness using the Li method was observed for softer coatings on harder and stiffer substrates such as sol-gel coatings on glass [3]. After correcting their results for crack geometry [45], a reasonable agreement can be

Table 1
The energy release rates and toughness calculated for the solar control coating components investigated in this study based on radial through-thickness fracture.

	Energy release rate of coating (J/m^2) by the W_t–dp model	Toughness of coating K_{IC} (MPa $\sqrt{m}$)	
		W_t–dp model	Conventional indentation model
400 nm TiO_xN_y top layer single layer	24.4 ± 1.4	1.8 ± 0.2	0.9 ± 0.1
240 nm ITO top layer multilayer stack	36.3 ± 8.2	2.2 ± 0.3	0.9 ± 0.1
400 nm ITO top layer multilayer stack	32.7 ± 4.4	2.1 ± 0.2	0.7 ± 0.1
400 nm TiO_xN_y top layer multilayer stack	24.1 ± 7.8	1.8 ± 0.2	1.0 ± 0.1
400 nm SnO_2 top layer multilayer stack	29.3 ± 9.8	1.9 ± 0.3	1.3 ± 0.1

achieved. The method thus does depend on the detailed formation mechanism of the crack and how this relates to the load–displacement curve – it is essential to stop the indentation cycle soon after the first pop-in event and then use post facto microscopy to determine crack patters if reliable data is to be determined.

The W_t–dp method proposed here can be used to evaluate the toughness using different types of crack such as delamination, radial cracks, picture frame cracks, chipping etc. given there is a feature in the load–displacement curve or W_t–displacement curve which is associated with fracture. The disadvantage of W_t–dp method is that the two-step extrapolation process may lead to more fitting errors. However, careful fitting techniques can reduce such fitting errors and make the results more physically reasonable.

3.2.2. Energy based model in the case of no obvious feature in the load–displacement curve

All the energy based models so far depend upon features in the load–displacement curve associated with fracture, otherwise, no slope change or jump in the plot of W_{irr} versus P or W_t–dp can be observed. However, as an example, in the case of solar control coatings on glass indented by a Berkovich indenter, a number of picture-frame cracks have been observed in the scanning electron microscope (SEM) whilst no obvious slope change or excursion has been found in the load–displacement curve even at the highest load applied by the Nanoindenter II (500 mN; Fig. 7). Similar phenomena have also been found for SiC or low-k dielectric coatings on Si in [46]. A question therefore arises if the fracture toughness can still be determined by an energy approach if the onset of fracture does not result in a feature in the load–displacement curve.

This issue has been address by Chen and Bull [8] in the following manner. The work of indentation can be written in the following form,

$$W_{tot} = W_P + U_{fra} + W_e + W_{other} \tag{13}$$

where W_{tot} is the total work, W_P is work of plastic deformation, W_e is work of elastic deformation, U_{fra} is the fracture dissipated energy, and W_{other} represents other items such as the heat dissipated during indentation, the energy dissipated in creep and microcracking. The sum of all the other items except W_e in Eq. (13) is the irreversible energy W_{irr} (here, we ignore any reversible plastic behaviour). Given an indentation procedure, we can easily measure W_{tot} and W_e, and, if we can find some procedure to determine W_P and W_{other} then the fracture dissipated energy U_{fra} can be obtained. In the following, one way to achieve this target is explained.

Imagine a load–displacement curve which has the following features: (1) impose the influence of cracking on the mechanical properties of the whole coated system after cracking to the whole loading part, namely, averaging the crack influence on the plastic and elastic deformation over the whole loading curve. This is reasonable if E/H remains almost constant despite the presence of fracture and the picture frame cracking appears and propagates during loading in our coated system as is usually observed; (2) this imaginary loading curve is an ideal loading curve without any new surface created for fracture; (3) it has the same total work to the measured load–displacement curve because the fracture events only convert some stored elastic energy into irreversible work under displacement control. The relationship between the real and imaginary curves is shown in (Fig. 8).

Since we averaged the fracture influence on the elastic–plastic deformation of the whole system in the indenting procedure, the work of plastic deformation (W_P) is equal in the two cases. For the ideal curve constructed here, the work of plastic deformation can be approximately determined based on the relationship between total work and plastic work by Cheng et al. [47]. However, there is always some deviation between the numerical fitting and the actual experiment data – at the high loads investigated here this is dominated by deformation processes in the substrate. Therefore, we analyse the uncoated substrate to determine the W_{other} term. Now W_{fra} can be obtained using Eq. (13); this represents the energy dissipated in the creation of new crack surface. Ideally, this approach can separate the influence of elastic–plastic deformation from fracture for coated systems with features similar to what has been described here. It can be also applied to brittle bulk materials given the condition that measurable cracking occurs and the fracture does not lead to a discontinuity in the load–displacement curve.

Using this method the toughness values for 400 nm SnO_2 and 240 ITO on glass are 1.6 ± 0.3 MPa $\sqrt{m}$ and 2.2 ± 0.5 MPa $\sqrt{m}$, respectively, in very good agreement with our previous reported values of 1.9 ± 0.3 MPa $\sqrt{m}$ and 2.2 ± 0.3 MPa $\sqrt{m}$ respectively [10]. It is necessary to point out that thermal drift needs to be strictly corrected if this method is adopted because this method considers the whole cycle of the indentation so that effects such as drift or creep will have

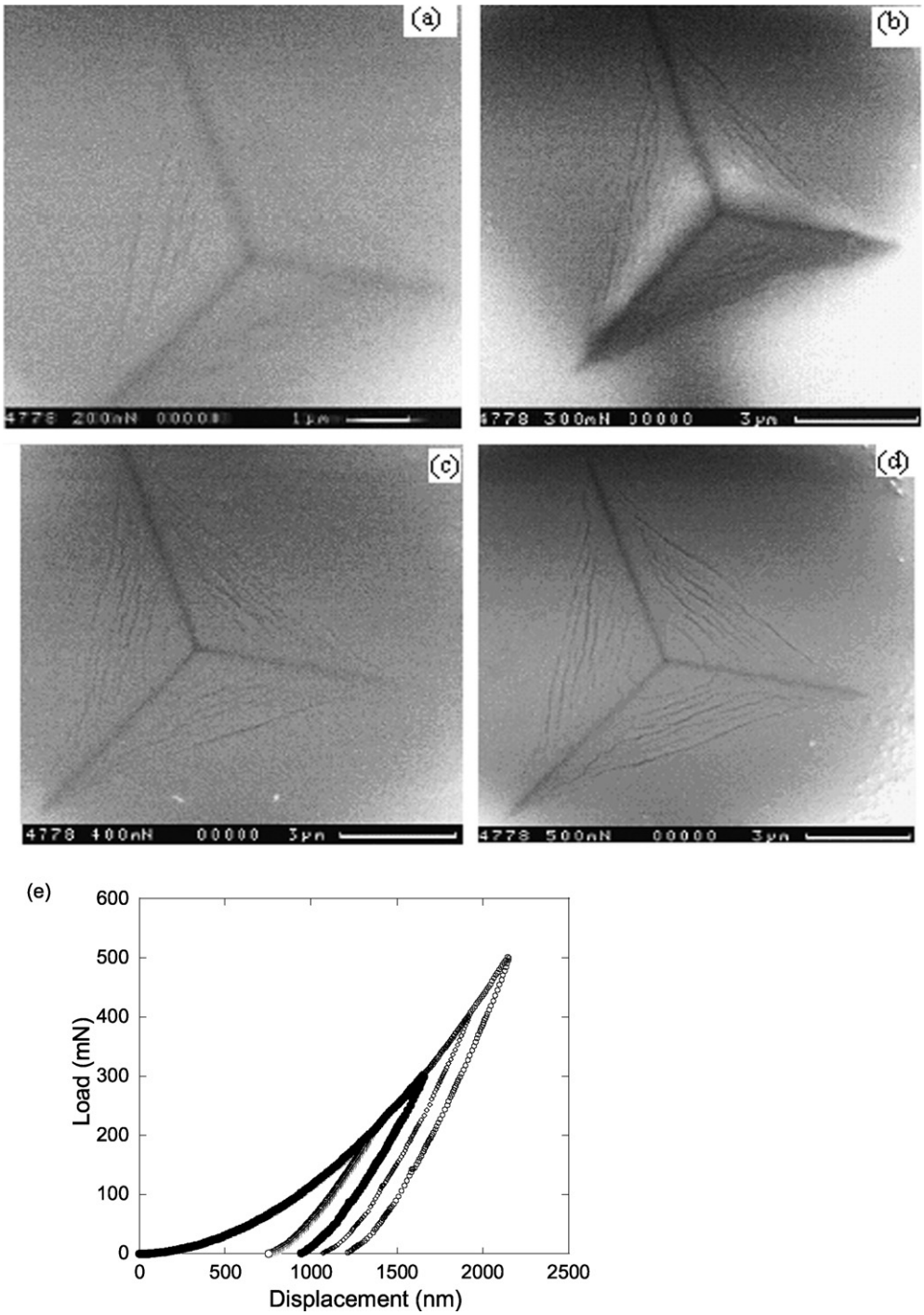

Fig. 7. Scanning electron micrographs of picture frame cracking produced by a Berkovich indenter in 400 nm ZnO coated architectural glass (a) 200 mN, (b) 300 mN, (c) 400 mN and (d) 500 mN peak load. (e) Associated load–displacement curves showing no features in the loading curve associated with fracture.

a significant influence on the results. It is not expected that this method will work in the case where a step or load drop is observed in the load–displacement curve, however, reasonable results can obtained in some coated systems despite a relatively big step in the load–displacement curve [30].

In summary, using stress-analysis in combination with empirical fitting allows the K_{IC} of a coating to be estimated by nanoindentation without analysing the load–displacement curve. This does not require the radial fracture to occur and propagate during the loading cycle. However, the energy-based models usually require the propagation of fracture to cease

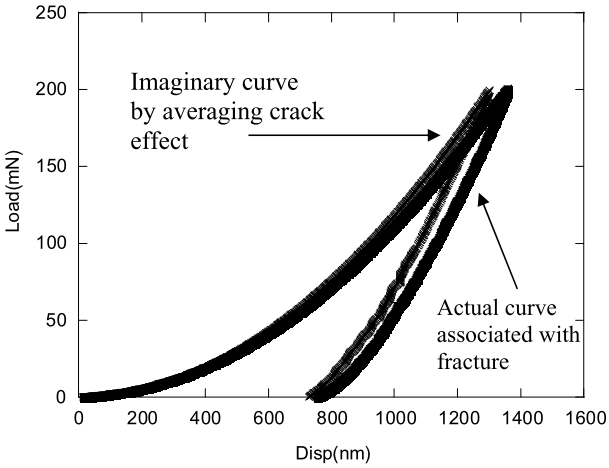

Fig. 8. Schematic explanation of the difference between an ideal and measured load–displacement curve for the measurement of irreversible work in picture frame cracking.

Table 2
Structure of the multilayer coatings investigated.

Position in the coating stack	Layer material	Nominal thickness (nm)
Outermost barrier coating	TiO_xN_y	10
Outer AR coating	SnO_2	40
Protective layer	ITO	2
Wavelength selective layer	Silver	10
Inner AR layer	ZnO	10
Inner barrier layer	TiO_xN_y	20
Substrate	Float glass (air side coated)	42 000 000

during loading. Stress-based models are limited to a single crack type and cracking mechanism. In contrast, the energy-based models are independent of the indenter geometry and crack pattern, given that the specific conditions outlined above can be satisfied.

4. Size effects in fracture toughness for oxide coatings on architectural glass

4.1. Coatings investigated

Experiments were carried out on float glass, coated with the main layers in a multilayer stack of silver and metal oxides in a solar control configuration. A commercial coating consists of a 10 nm silver layer surrounded by SnO_2 and ZnO anti-reflection coatings and TiO_xN_y barrier layers; the layer structure and nominal coating thicknesses are presented in Table 2. A thin conducting ITO layer is used to prevent the silver layer from oxidation during the subsequent deposition of tin oxide. For the purposes of fracture and plasticity assessment of the individual oxide layer materials the previous coating layers were deposited according to the solar control coating design in Table 2 but the final coating layer was deposited to a range of thicknesses from 100 to 400 nm. This should ensure a similar microstructure is tested in each case.

The coatings were produced by sputtering in a commercial coating plant at Pilkington Technical Centre (Lathom, UK) using the same process parameters as used for commercially available solar control coatings from the same manufacturer (available with the trade name Optitherm).

4.2. Indentation testing approach

Indentation experiments were performed using a Hysitron Triboindenter fitted with a new Berkovich indenter (tip-end radius 100 nm) for plasticity assessment and a new cube corner indenter (tip end-radius 40 nm) for fracture assessment. Tests were performed under displacement control since this has been shown to generate accurate fracture data in such coatings [10]. The system hardness and elastic modulus were determined by the standard Oliver and Pharr method [48] since these materials do not display significant pile-up or sink-in. Measurements were made at a range of contact scales in order to allow the extraction of coating-only properties using the extrapolation methods outlined in ISO 14577 [49].

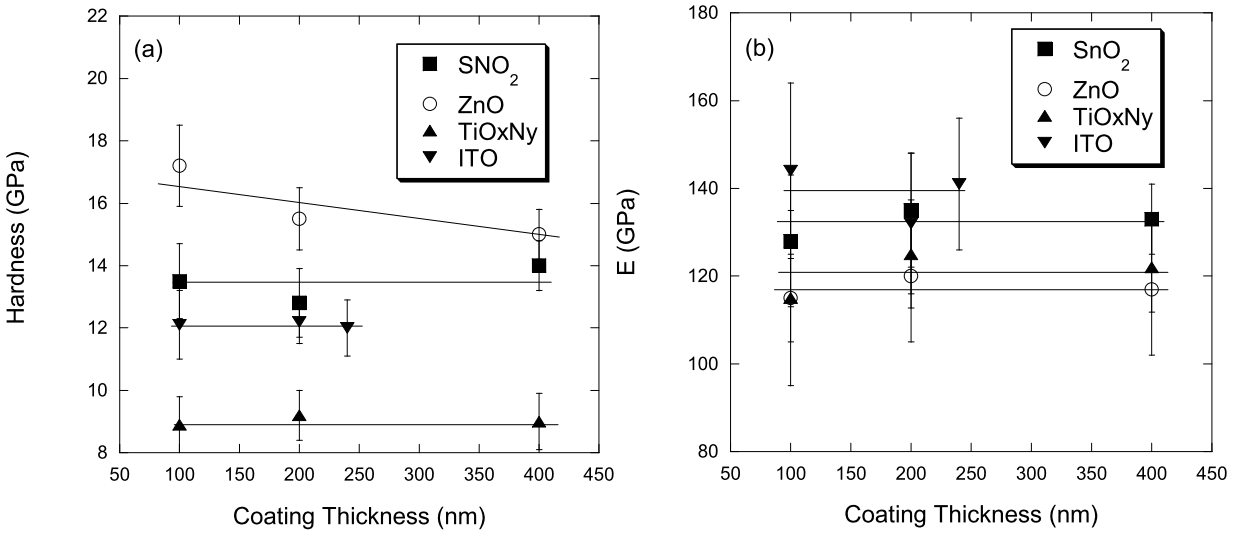

Fig. 9. (a) Hardness and (b) Young's modulus determined by nanoindentation as a function of coating thickness.

4.3. Size effects in plasticity

Hardness (and elasticity) data was obtained at a range of contact scales for coatings in the thickness range 100–400 nm and extrapolated to zero thickness to give an indication of the coating only properties (Fig. 9). For most of the oxide coatings studied there is no appreciable size effect, though for zinc oxide the hardness does increase at lower coating thickness. This is probably related to the fact that all the deposited oxide coatings are poorly crystalline except for the ZnO and scale-dependent plasticity mechanisms, such as geometrically necessary dislocations [32,50] require the presence of dislocations on well-defined slip planes which are not present in amorphous layers.

4.4. Size effects in fracture

Cube corner indentations have been performed in all oxide coatings tested here and generate fracture in the coatings. Depending on the coating material both picture frame and radial cracks were observed to form. When radial cracks were observed for the TO_xN_y, SnO_2 and ITO layers there were well defined features in the load–displacement curve (load drops since under displacement control) and the wp-dp method could be used for analysis. At higher loads in these coatings picture frame cracks formed and once these were well-established, the picture frame crack method could be used to determine critical strain energy release rates. For ZnO layers this is the only practicable way to obtain such data. There was reasonable agreement between the toughness values calculated by either approach. For coatings in the thickness range 100–400 nm no size effects were observed (Fig. 10). Assuming pure mode I loading the critical strain energy release rates can be converted to fracture toughness values using

$$K_{IC} = \sqrt{EG_c} \tag{14}$$

Results of this calculation are presented in Table 3 and are comparable to data from bulk samples of the same materials obtained using conventional toughness tests.

Some workers have reported size effects in the fracture of oxide nanoparticles (e.g. [50]) but these are typically much less than 100 nm in diameter. The mechanisms used to describe such size-dependent fracture events are often related to the effects of local plasticity in the region of the crack tip – given the lack of size effects in plasticity in these predominantly amorphous coatings the lack of a size effect in fracture is therefore not surprising.

Differences in fracture behaviour will depend on the distribution of defects in the coating as well as on the fracture toughness. Careful analysis of the coatings by AFM and transmission electron microscopy reveals, poorly crystalline layers with few defects and none of the dislocations that are required for dislocation shielding based models for size effects in toughness [51]. There thus remains the question of what is the critical defect responsible for fracture.

The critical crack size, c, can be estimated from

$$K_{IC} = \sigma\sqrt{\pi c} \tag{15}$$

where σ is the tensile stress opening the crack. This stress will be the combination of the residual stress in the coating and the stress introduced by the indentation process. Table 3 shows measured values of residual stress in the coating (using the curvature method [52]). Table 3 also shows the stresses in the coating at the location of failure determined by finite element analysis of an indenter pressed into the coated sample with the fracture load; for details of the modelling approach

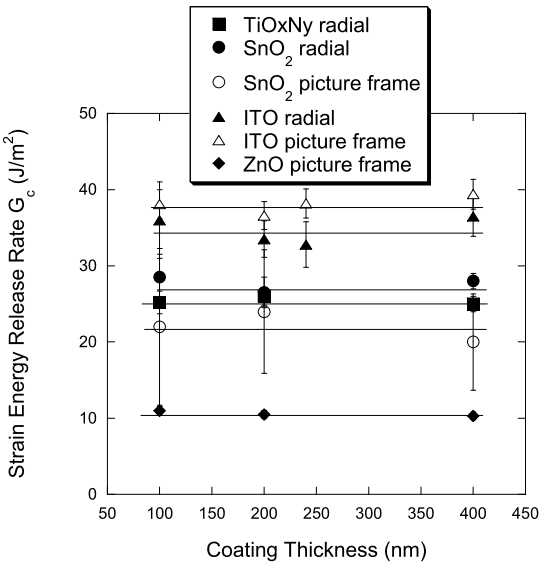

Fig. 10. Strain energy release rate as a function of coating thickness for oxide coatings on glass determined by the wp–dp and picture frame crack methods.

Table 3
Stresses, fracture toughness and critical crack size for the 400 nm thick coatings investigated in this study.

Coating	Residual stress, σ_r (GPa)	Indentation stress, σ_a (GPa)	Coating Youngs modulus, E (GPa)	Coating fracture toughness, K_{IC} (MPa m$^{1/2}$)	Critical crack size, c (nm)	Ra (nm)
TiO_xN_y	−0.2	12.2	122	1.8	7.2	9.1
ZnO	−1.0	11.7	117	1.1	3.4	12.7
ITO	−3.0	13.1	141	2.2	15.1	6.6
SnO_2	−3.0	13.3	133	1.9	10.8	8.6

see [53,54]. The critical crack sizes determined using Eq. (15) in this table are of a similar size to the surface roughness of the coatings and it is probable that the cracks are formed from surface roughness features. Since the surface roughness of the coatings does not vary appreciably with coating thickness there is no size effect in fracture behaviour introduced by changing defect distributions.

5. Conclusions

There are numerous methods which can be used to assess the coating toughness or adhesion between a coating and its substrate. There are no universal coating fracture or adhesion tests but quantitative values are available from some tests in particular situations. In this paper, a critical review has been made on the main indentation-based methods which are most suitable for thin coated systems. The selection of different models to analyse the data produced from nanoindentation load–displacement curves depends on the type of failure observed. High resolution microscopic analysis of the impression to analyse fracture mechanisms is an essential part of toughness calculations if reliable data is to be obtained.

Energy-based methods can be used to assess the fracture toughness of very thin oxide coatings on architectural glass based on either radial or picture-frame cracking. For coating thicknesses between 100 and 400 nm there are no appreciable size effects in fracture toughness; At the contact stresses required to create fracture it is the distribution of defects which controls fracture behaviour since the critical crack size is comparable to the surface roughness of the coating.

Acknowledgements

This work was supported by EPSRC through the multiscale modelling initiative.

References

[1] B.R. Lawn, A.G. Evans, J. Am. Ceram. Soc. 63 (1980) 574.
[2] G.R. Anstis, P. Chantikul, B.R. Lawn, D.B. Marshall, J. Am. Ceram. Soc. 64 (1981) 533.
[3] J. Malzbender, G. de With, J.M.J. den Toonder, Thin Solid Films 366 (2000) 139.
[4] R.F. Cook, G.M. Pharr, J. Am. Ceram. Soc. 73 (1990) 787.
[5] J. Jang, S. Wen, M.J. Lance, I.M. Anderson, G.M. Pharr, Mater. Res. Soc. Symp. Proc. 795 (2004), U8. 15.1.

[6] D.S. Harding, W.C. Oliver, G.M. Pharr, Mater. Res. Soc. Symp. Proc. 356 (1995) 663.
[7] G.M. Pharr, Mater. Sci. Eng. A 253 (1998) 151.
[8] J. Chen, S.J. Bull, J. Phys. D: Appl. Phys. 40 (2007) 5401.
[9] X. Li, D. Diao, B. Bhushan, Acta Mat. 45 (1997) 4453.
[10] J. Chen, S.J. Bull, Thin Solid Films 494 (2006) 1.
[11] G.M. Pharr, D.S. Harding, W.C. Oliver, Mechanical Properties and Deformation Behaviour of Materials Having Ultra-Fine Microstructure, Kluwer Academic Press, Dordrecht, 1993, p. 449.
[12] T.W. Scharf, H. Deng, J.A. Barnard, J. Vac. Sci. A 15 (1997) 963.
[13] D.B. Marshall, A.G. Evans, Comm. Am. Ceram. Soc. (1982) C182.
[14] J. Malzbender, G. de With, J. Non-Cryst. Sol. 265 (2000) 51.
[15] D.B. Marshall, B.R. Lawn, J. Am. Ceram. Soc. 60 (1977) 86.
[16] M.L. Emiliani, J. Mater. Sci. 28 (1993) 5280.
[17] P. Kodali, K.C. Walter, N. Nastasi, Tribol. Int. 30 (1997) 591.
[18] D. Broek, Elementary Engineering Fracture Mechanics, Kluwer, Dordrecht, The Netherlands, 1997.
[19] J. den Toonder, J. Malzbender, G. de With, R. Balkenende, J. Mater. Res. 17 (2002) 224.
[20] M.T. Laugier, J. Mater. Sci. Lett. 6 (1987) 879.
[21] K. Nihara, R. Morena, D.P.H. Hasselman, J. Mater. Sci. Lett. 1 (1982) 13.
[22] T. Scholz, G.A. Schneider, J. Muñoz-Saldaña, M.V. Swain, Appl. Phys. Lett. 84 (2004) 3055.
[23] K. Tanaka, Y. Kitahara, Y. Ichinose, T. Iimura, Acta Metall 32 (1984) 1719.
[24] Y.G. Jung, A. Pajares, R. Banerjee, B.R. Lawn, Acta Mater. 52 (2004) 3459.
[25] J.S. Field, M.V. Swain, R.D. Dukino, J. Mater. Res. 18 (2003) 1412.
[26] J. Mencik, Mechanics of Components with Treated or Coated Surface, Dordrecht, Kluwer, 1996.
[27] D.B. Marshall, B.R. Lawn, J. Mater. Sci. 14 (1979) 2001.
[28] T.F. Page, S.V. Hainsworth, Surf. Coat. Technol. 61 (1993) 201.
[29] T. Fett, Computation of the crack opening displacements for Vickers indentation cracks, Report. No. FZKA 6757, Forschungszentrum Karlsruhe, Karlsruhe, Germany, 2002.
[30] J.J. Kruzic, R.O. Ritchie, J. Am. Ceram. Soc. 86 (2003) 1433.
[31] R. Briard, C. Heitz, E. Barthel, J. Non-Cryst. Sol. 351 (2005) 323.
[32] S.J. Bull, Z. Metall. 94 (2003) 787.
[33] S.J. Bull, T.F. Page, E.H. Yoffe, Phil. Mag. Lett. 59 (1989) 281.
[34] B.R. Lawn, Fracture of Brittle Solids, 2nd ed., Cambridge University Press, Cambridge, 1993.
[35] Z. Burghard, A. Zimmermann, J. Rödel, F. Aldinger, B.R. Lawn, Acta Mater. 52 (2004) 293.
[36] P. Chantikul, G.R. Anstis, B.R. Lawn, D.B. Marshall, J. Am. Ceram. Soc. 64 (1981) 539.
[37] D.B. Marshall, B.R. Lawn, A.G. Evans, J. Am. Ceram. Soc. 65 (1982) 561.
[38] M.T. Laugier, J. Mater. Sci. Lett. 6 (1987) 768.
[39] R.D. Dukino, M.V. Swain, J. Am. Ceram. Soc. 75 (1992) 3299.
[40] X. Li, B. Bhushan, Thin Solid Films 315 (1998) 214.
[41] J. Malzbender, G. de With, Surf. Coat. Technol. 135 (2000) 60.
[42] J. Chen, S.J. Bull, Mat. Res. Soc. Symp. Proc. 890 (2006) 57.
[43] R.N. Stevens, F. Guiu, Proc. Roy. Soc. Lond. A 435 (1991) 169.
[44] J.E. Field, C.S.J. Pickles, Diamond and Related Materials 5 (1996) 625.
[45] M.S. Hu, M.D. Thouless, A.G. Evans, Acta Mater. 36 (1988) 1301.
[46] A.A. Volinsky, J.B. Vella, W.W. Gerberich, Thin Solid Films 429 (2003) 201.
[47] Y.-T. Cheng, Z. Li, C.-M. Cheng, Phil. Mag. A 82 (2002) 1821.
[48] W.C. Oliver, G.M. Pharr, J. Mater. Res. 7 (1992) 1564.
[49] ISO14577 part 4 (2007).
[50] W.W. Gerberich, W.M. Mook, C.B. Carter, R. Ballinari, Int. J. Fracture 148 (2007) 109.
[51] Y. Katz, R. Keller, H. Huang, W.W. Gerberich, Metall. Trans. A 24 (1993) 343.
[52] J.A. Sue, in: ASM Handbook, vol. 5: Surface Engineering, ASM International, Metals Park, Ohio, 1994, pp. 647–653.
[53] J. Chen, S.J. Bull, J. Mater. Res. 21 (2006) 2617.
[54] J. Chen, S.J. Bull, Thin Solid Films 517 (2009) 3704.